J Mater Sci (2011) 46:6508–6517
DOI 10.1007/s10853-011-5597-2

Effect of organoclay with various organic modifiers on the morphological, mechanical, and gas barrier properties of thermoplastic polyurethane/organoclay nanocomposites

Dekun Sheng · Juanjuan Tan · Xiangdong Liu · Pixin Wang · Yuming Yang

Received: 6 January 2011 / Accepted: 27 April 2011 / Published online: 21 May 2011

Abstract Thermoplastic polyurethane (TPU)/organoclay nanocomposites are prepared through a melt extrusion process. The TPU is combined with four differently modified organoclays, namely, I.28E, I.30P, I.34TCN, and I.44P. Wide-angle X-ray diffraction and transmission electron microscopy results show that the addition of I.34TCN and I.30P to TPU/organoclay nanocomposites results in the nearly exfoliated structures of the nanocomposites. Addition of I.28E leads to partially intercalated nanocomposites, whereas I.44P cannot disperse effectively in the nanocomposites. Organoclay can enhance the mechanical and gas barrier properties of TPU. The enhancement follows the order TPU/I.34TCN $\geq$ TPU/I.30P $>$ TPU/I.28E $>$ TPU/I.44P, which is consistent with the degree of dispersion and exfoliation of silicate layers. In addition, Fourier transform infrared absorption spectra show that more hydrogen bonding sites are introduced between the clay modifiers and TPU chains in the TPU/I.34TCN and TPU/I.30P nanocomposites; this has a positive impact on the dispersion of the organoclay and, consequently, the mechanical and gas barrier properties of the nanocomposites.

D. Sheng · J. Tan · X. Liu · P. Wang · Y. Yang (✉)
Key Laboratory of Polymer Ecomaterials, Changchun Institute of Applied Chemistry, Chinese Academy of Sciences, Changchun 130022, People's Republic of China
e-mail: ymyang@ciac.jl.cn

D. Sheng · J. Tan · X. Liu
Graduate School of the Chinese Academy of Sciences, Beijing 100049, People's Republic of China

Introduction

In recent years, polymer/clay nanocomposites have attracted much attention for their great importance in fundamental research and industrial applications. Compared with the polymer matrix, polymer/clay nanocomposites provide significant improvements in mechanical, thermal, and physicochemical properties [1]. To date, numerous polymer matrices have been studied in clay-based nanocomposites, including polyimide [2], polystyrene [3], poly(lactic acid) [4], poly(ethylene-co-vinyl alcohol) [5], natural rubber [6], poly(methyl methacrylate) [7], polypropylene [8], and polyethylene [9].

Clay consists of naturally occurring layered silicates. The thickness of each layer is $\sim$1 nm, and its lateral dimensions are typically within 20–1000 nm. The stacking of the layers forms a gallery ($\sim$1 nm thickness) between layers [10]. The silicate layers of clay usually contain hydrated Na^+ or K^+, which render them highly hydrophilic and incompatible with most organic polymers. Therefore, the silicate layers must be modified to increase their hydrophobicity. The modified organic clay is known as organoclay. The most popular method used for clay modification is exchange of hydrated cations with organic modifiers such as alkylammonium cations. Some alkylammonium cations with functional groups may react with the polymer matrix, which would improve the strength of the interface between the inorganic layer and the polymer. In some cases, these functional groups play important roles in the dispersion of the silicate layers. The high compatibility between the functional group and the polymer chains can result in a high degree of exfoliation of the polymer matrix [11–14]. The separated silicate layers enable high interfacial interaction between polymer chains and thereby provide higher mechanical reinforcement, impermeability,

and thermal stability [15]. Moreover, these organic modifiers can enhance the interlayer *d* spacings, lower the surface energy of the inorganic host, and improve the wetting characteristics of the polymer [16, 17].

Thermoplastic polyurethane (TPU) is composed of alternating soft and hard segments. The soft segment is a high-molecular weight polyester or polyether diol, and the hard segment consists of diisocyanate and chain extender (low molecular weight diol or diamine). Wang and Pinnavaia first reported a polyurethane/organoclay composite in 1998 [18]. Since then, many studies have focused on approaches to introduce silicate layers into the TPU matrix to improve its properties [19, 20]. Various types of organoclays and organic modifiers have been used [21]. The organic modifiers with long alkyl chains and hydroxyl groups (such as commercial organoclay C30B or I.34TCN) can almost fully exfoliate silicate layers in the TPU matrix, and increase the tensile strength, modulus, and optical clarity by more than 100% compared with pure TPU [22].

The aim of this study was to investigate the effects of clay with different organic modifiers and composition on the morphological, mechanical, and gas barrier properties of TPU. Four types of organoclay, namely, I.28E, I.30P, I.34TCN, and I.44P, with various organic modifiers (Fig. 1) were used. A number of studies have been done on I.34TCN and I.44P [23], but few have focused on I.28E and I.30P in TPU/clay nanocomposites. Polymer nanocomposites based on TPU and the four types of organoclay were prepared through melt extrusion in a twin-screw extruder. The morphology of the nanocomposites was characterized by wide-angle X-ray diffraction (WAXD) and transmission electron microscopy (TEM). The static and dynamic mechanical properties of the nanocomposites were examined by tensile testing and dynamic mechanical analysis (DMA), respectively. Analysis of the oxygen gas permeability was performed using a film-package permeability tester. Fourier transform infrared (FTIR) spectroscopy was done to investigate the relationship between the properties and hydrogen bonding involved in the TPU/organoclay nanocomposites.

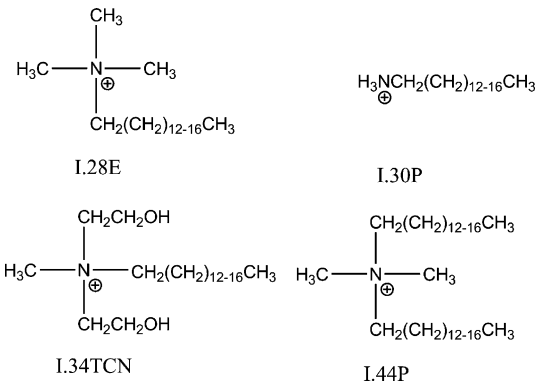

Fig. 1 Molecular structures of the organic modifiers

Experimental

Materials

Thermoplastic polyurethane (TPU, Estane® 58315; 85A Shore hardness) was provided by Lubrizol Advanced Materials, Inc. The commercial organoclays, Nanomer I.30P, I.28E, I.34TCN, and I.44P, were obtained from Nanocor, Inc. These organoclays were composed of natural montmorillonite modified with organic modifiers (Fig. 1). The samples I.28E and I.30P were clays modified with octadecyl trimethyl quaternary ammonium ion and octadecan-1-aminium ion, respectively; I.34TCN was modified by methyl-bis-(2-hydroxyethyl) hydrogenated tallow quaternary ammonium ion (tallow: 65% C18, 30% C16, and 5% C14); I.44P was modified with dimethyl dihydrogenated tallow quaternary ammonium ion.

Sample preparation

The organoclays and TPU were dried at 90 and 60 °C under vacuum for 24 h, respectively. They were melt-extruded using a co-rotating intermeshing twin-screw extruder (Haake Rheomex PTW 24/40P, Thermo Electron Corp., Hamburg, Germany). The extrudates were then cooled in water at the die exit, dried by air, and then cut into pellets. The thermal profile was 160–200 °C, and the screw speed was set at 60 rpm. The neat polymer used as reference material was extruded under the same conditions. The extruded blends were dried and annealed at 100 °C overnight, which led to isotropy in the composites and formed a network between the silicate layers and TPU matrix [24]. The TPU/organoclay nanocomposites were prepared with 1, 3, 5, 7, and 10 wt% organoclay. All blends were pressed into films (1-mm thickness) at 190 °C for 3 min, which were then quenched to room temperature between two thick metal blocks. A single-screw extruder (Haake Rheomex 252P, Thermo Electron Corp, Hamburg, Germany) equipped with a blowing film line was used to produce the films.

Characterization

WAXD experiments were performed using a Rigaku D/Max-II B X-ray diffractometer with a Cu anode. The instrument was operated at 40 kV and 200 mA; 2θ measurements from 2.5° to 10° were done at a scan rate of 1°/min. The organoclay powder and the TPU/organoclay films were analyzed at ambient conditions.

The dispersions of silicate layers were observed using a transmission electron microscope (JEOL JEM-1011). The nanocomposite specimen for TEM observations (50–70-nm thickness) was prepared under cryogenic conditions using a Leica ultramicrotome.

Dynamic mechanical tests were performed on a DMA/SDTA861^e (Mettler Toledo) in shear mode. The samples were cut on the 1-mm thick polyurethane films with a diameter of 10 mm. These were then analyzed under a nitrogen atmosphere from −100 to 150 °C, at 3 °C/min heating rate, 1 Hz frequency, and ∼0.2% initial strain.

The static mechanical properties of the samples were determined on an Instron 1185 tensile testing machine at a rate of 50 mm/min at room temperature. Oar-shaped specimens with 20.0-mm gauge length and 4.0-mm width were cut from the 1-mm thick films. At least five samples of each type were drawn to fracture.

The oxygen gas permeability through the films of TPU and the nanocomposites was measured using a Labthink VAC-V2 film-package permeability tester. The permeability was expressed as the volume rate of gas penetrating a unit thickness of film at constant pressure, humidity, and temperature. The tests were performed at 23 °C and 0% relative humidity using high-purity (>99.9%) oxygen gas. The tests were performed according to GB/T 1038-2000 (China).

FTIR spectra were recorded on a Bruker Vertex70 spectrophotometer at 2 cm^{-1} resolution.

Results and discussion

Morphology of the nanocomposites

WAXD is a powerful technique for studying clay dispersion in polymer/organoclay nanocomposites. It could be used to determine the distributions of d spacings within the clay silicate layers and/or agglomerates. The powder diffractograms of the four organoclays were compared with those of the corresponding nanocomposite films (Fig. 2). The (001) basal-plane spacing (d_{001}) of I.28E, I.30P, I.34TCN, and I.44P were 2.67, 2.16, 1.87, and 2.54 nm, respectively; these indicates the differences in thickness of the organic layers between the silicate layers. After melt extrusion, the d_{001} WAXD peak of the clays shifts to a smaller angle or disappears, which indicates the occurrence of intercalation or exfoliation of silicate layers. The intensity of the d_{001} WAXD peaks of the clays increases with clay loading, which suggests the decreasing dispersion of silicate layers. Thus, the organoclay silicate layers tend to form agglomerates rather than exfoliate. For the four types of TPU/organoclay nanocomposites with 10 wt% clay loading, the interlayer distance of the silicate layers calculated from the WAXD reflections increases to 3.36, 3.17, 3.15, and 3.06 nm for I.28E, I.30P, I.34TCN, and I.44P, respectively. Narrowing of the characteristic d_{001} WAXD peak of TPU/I.44P, TPU/I.28E, and TPU/I.30P nanocomposites with 10 wt% clay loading indicates

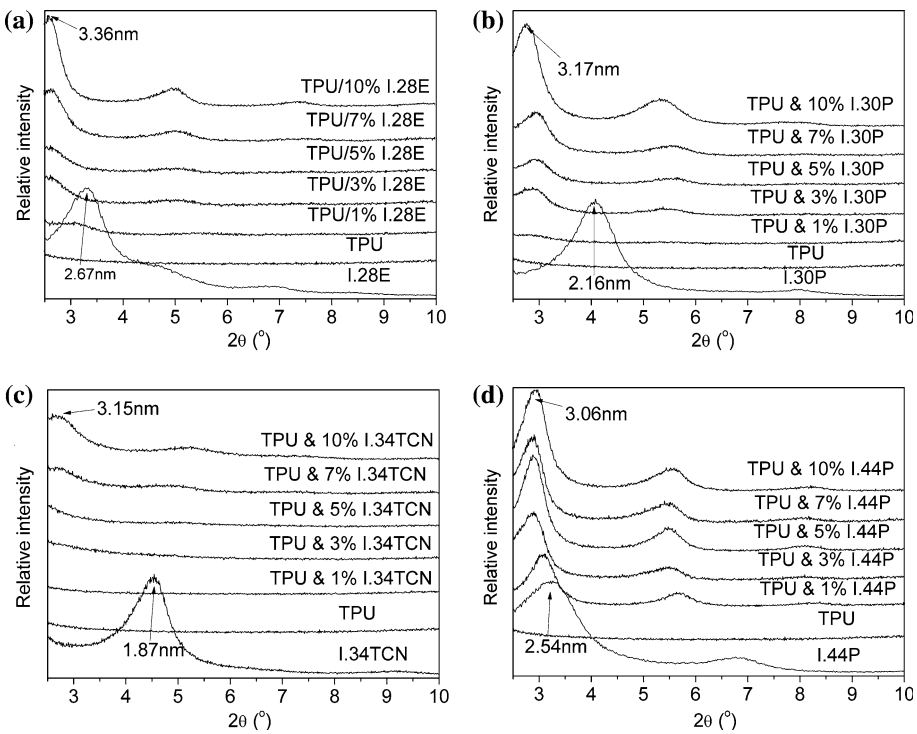

Fig. 2 WAXD patterns of TPU nanocomposites with **a** I.28E, **b** I.30P, **c** I.34TCN, and **d** I.44P

intercalation. In addition, the peak displacement between 2θ values of 5° and 6° is related to the presence of natural montmorillonite in the samples even after organic modification [25]. For the TPU/I.34TCN nanocomposites with low clay contents, the characteristic clay peaks are widened and are nearly undetectable. This indicates that the silicate layers are well distributed and completely exfoliated.

One of the difficulties in studying nanocomposites is that no single characterization method can adequately describe the state of the clay dispersion in the nanocomposites [26]. Thus, TEM studies are carried out to further confirm the dispersion states of the TPU/organoclay nanocomposites. Figure 3 shows TEM images of an ultrathin section of each TPU/organoclay nanocomposite with 3 wt% clay. The dark lines ($\sim$300 nm in length) are silicate layers. The longest and thickest agglomerates of the silicate layers were observed in the TPU/I.44P nanocomposite with a gallery of 3–4 nm. In the TPU/I.28E nanocomposite, some individual and agglomerated silicate layers were observed. In the TPU/I.34TCN and TPU/I.30P nanocomposites, most silicate layers existed as individual or double layers. Figure 4 shows the TEM images of the four TPU/organoclay nanocomposites with 7 wt% clay. Compared with nanocomposites with 3 wt% clay, more and larger agglomerates were observed. This indicates the decreasing dispersion of silicate layers with an increase in clay loading. Furthermore, organoclay silicate layers are dispersed better in the TPU/I.34TCN and TPU/I.30P nanocomposites than in the TPU/I.28E and TPU/I.44P nanocomposites with 7 wt% clay. This is consistent with the results of the nanocomposites with 3 wt% clay loading.

The better dispersion and higher degree of exfoliation of silicate layers in the TPU/I.34TCN and TPU/I.30P nanocomposites are probably due to the strong interfacial interaction between the silicate layers and TPU matrix. The hydroxyl or ammonium group of I.34TCN and I.30P linked to the silicate layer surface can form strong interfacial interaction, such as hydrogen bonding with the TPU macromolecular chains [27]. Based on the interactions between the modified silicate surfaces and the surrounding polymer melt, the polymer has to penetrate the space between two silicate layers from an outer edge and then diffuse toward the center of the gallery. Thus, the polymer and silicate layer surface attract each other. Although the TPU chains

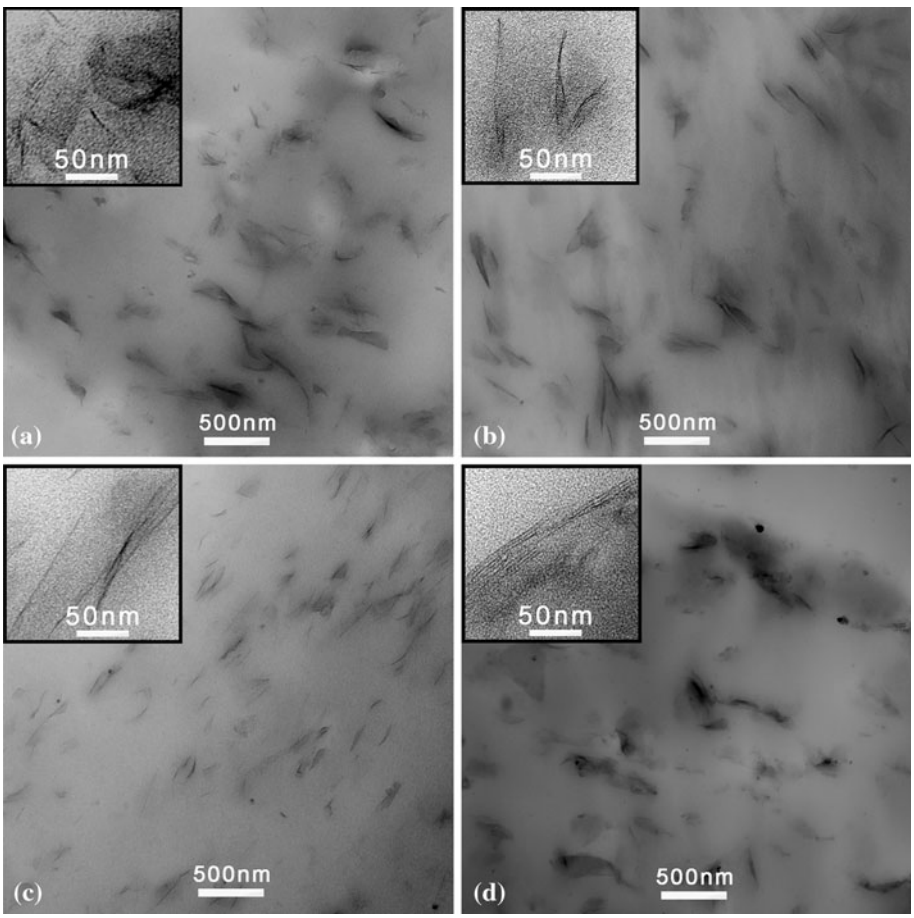

Fig. 3 TEM images of TPU nanocomposites with 3 wt% of **a** I.28E, **b** I.30P, **c** I.34TCN, and **d** I.44P

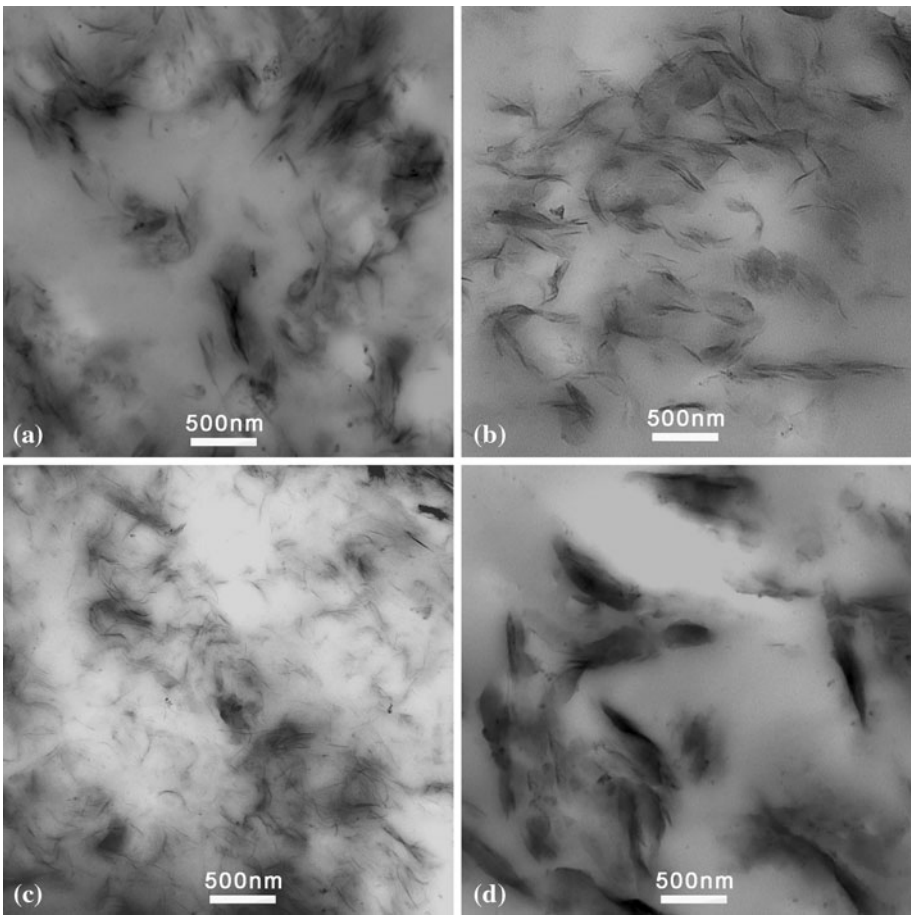

Fig. 4 TEM images of TPU nanocomposites with 7 wt% of **a** I.28E, **b** I.30P, **c** I.34TCN, and **d** I.44P

highly attract the silicate layer surfaces, the adhesive role of the polymer chains tends to reduce the van der Waals force between silicate layers. This allows complete dissociation of organoclay silicate layers, which leads to effective diffusion of polymer chains into the gallery and formation of composites with exfoliated morphologies [28, 29].

Dynamic mechanical properties

The dynamic mechanical property of the TPU/organoclay nanocomposites as a function of temperature was measured using DMA, and was compared with those of neat polyurethane. The temperature dependence of the loss factor (tan δ) and the storage shear modulus (G') are shown in Figs. 5 and 6, respectively. The plot of tan δ versus temperature of pure TPU shows a prominent peak at around −30 °C. This transition corresponds to the soft segment relaxation associated with the glass transition of the TPU amorphous phase. However, the peak for the relaxation corresponding to the glass transition temperature (T_g) of the TPU/organoclay nanocomposites appears at a higher temperature. Moreover, the addition of clay broadens the tan δ peak. The T_g and full width at half maximum (FWHM) of tan δ of the nanocomposites are presented in Table 1. Both TPU/I.30P and TPU/I.34TCN have higher T_g and broader tan δ peaks compared with those of TPU/I.28E and TPU/I.44P. The broader width of the tan δ peak implies higher density of the physically cross-linked network in the TPU matrix formed by hydrogen bonding of TPU chains or silicate layers; this strongly restricts the polymer segment motions and causes a higher T_g [30]. Moreover, the increase in tan δ value above T_g with the addition of organoclay is due to the enhancement of the damping properties of the TPU matrix by silicate layers. The slight drop of T_g with higher organoclay loading is probably due to the increase in intercalation of the TPU chains. The electrostatic attraction between the two adjacent silicate layers weakens because of the intercalation of TPU chains into their gallery. This causes the layers to slip easily under shear stress [31]. Therefore, the TPU matrix relaxation may be achieved at lower temperature, and thus reduce the T_g.

The value of G' above T_g is evidently enhances with increasing clay content. This indicates that the incorporation of organoclay reinforces TPU in the rubbery state. The reinforcement may be due to the stiffness of the silicate layers, as well as the combined effect of aspect ratio and

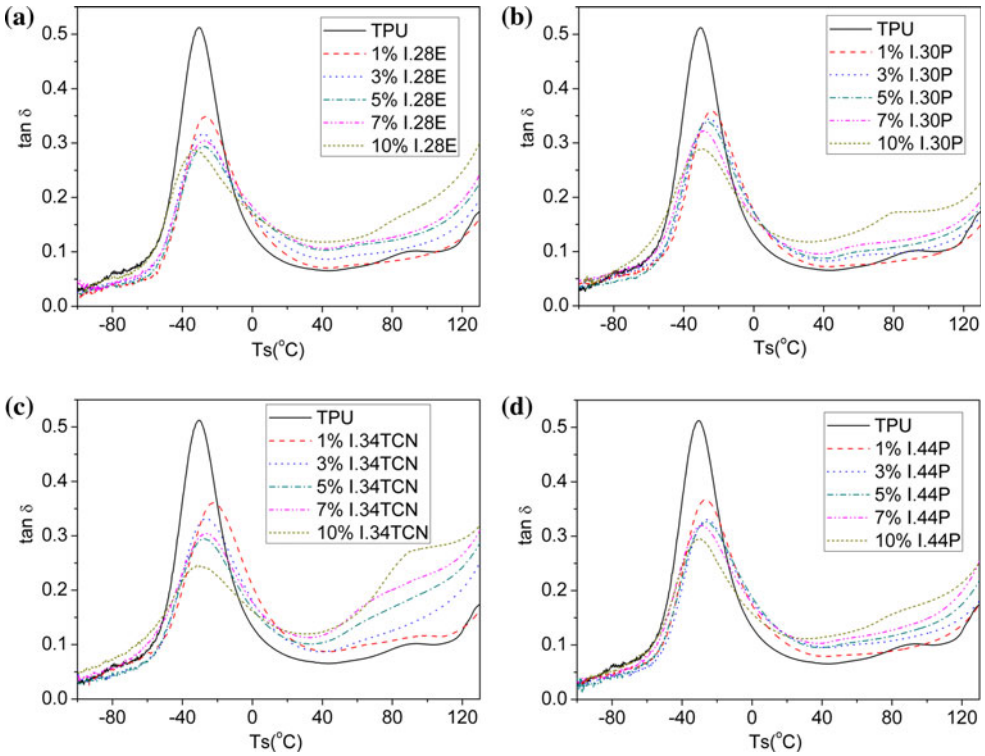

Fig. 5 Loss factors (tan δ) of the TPU nanocomposites with **a** I.28E, **b** I.30P, **c** I.34TCN, and **d** I.44P

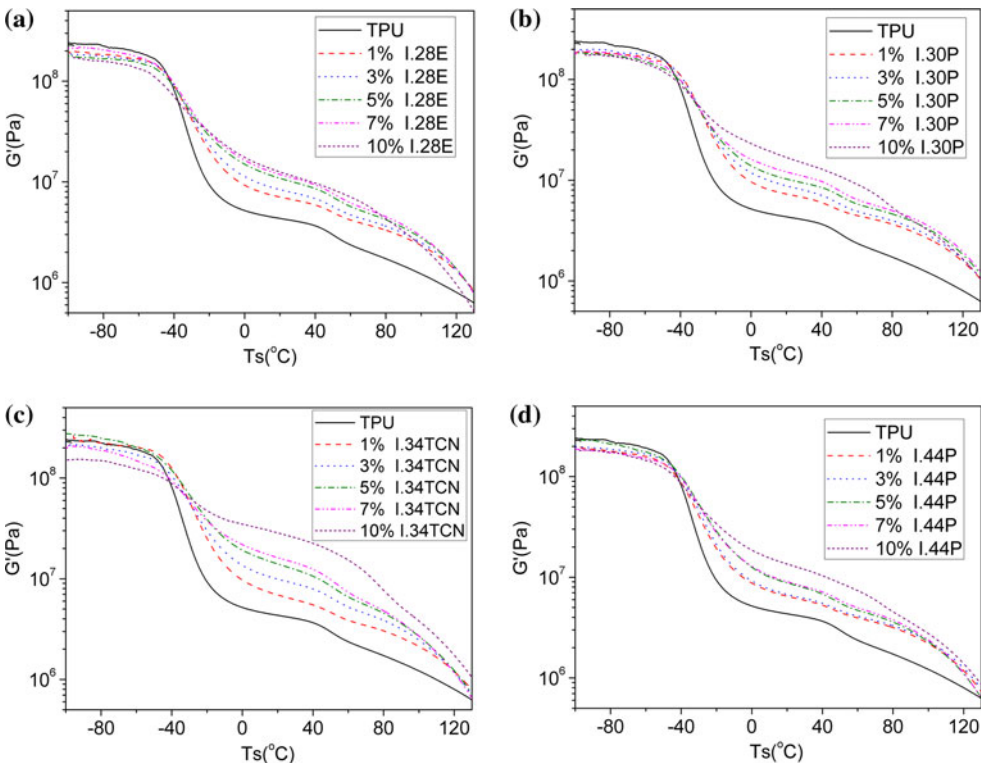

Fig. 6 Storage modulus of TPU nanocomposites with **a** I.28E, **b** I.30P, **c** I.34TCN, and **d** I.44P

the degree of silicate layer dispersion. Figure 7 shows that with 3 wt% organoclay loading, the TPU/I.34TCN and TPU/I.30P nanocomposites show higher values of G' compared with those of the TPU/I.28E and TPU/I.44P nanocomposites. This can be attributed to better exfoliation of the silicate layers in the TPU/I.34TCN and TPU/I.30P nanocomposites, which is consistent with the WAXD and TEM results.

Table 1 Glass transition temperature (T_g, °C) of TPU nanocomposites and FWHM (°C) of the loss factor peaks

	TPU		TPU/I.28E		TPU/I.30P		TPU/I.34TCN		TPU/I.44P	
	T_g	FWHM	T_g	FWHM	T_g	FWHM	T_g	FWHM	T_g	FWHM
	−30.88	26.88								
1 wt%			−26.18	33.78	−23.96	35.47	−22.54	37.50	−26.79	34.74
3 wt%			−28.67	35.54	−26.28	38.31	−25.50	39.48	−28.28	37.42
5 wt%			−29.14	36.73	−27.14	40.21	−27.56	39.63	−26.72	38.08
7 wt%			−27.4	37.68	−28.02	40.26	−26.82	40.28	−28.75	40.15
10 wt%			−32.44	39.14	−29.45	41.76	−29.63	44.98	−32.59	39.54

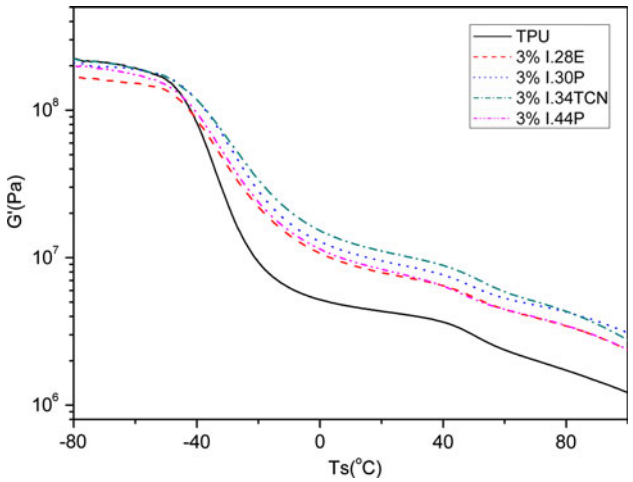

Fig. 7 Storage modulus of TPU nanocomposites with 3 wt% clay

Static mechanical properties

Figure 8 illustrates the tensile strength, elastic modulus, and elongation at break of the nanocomposites. The tensile strength and elongation at break of all nanocomposites first increase and then decrease with increasing organoclay content. The nanocomposites with 3 wt% organoclay content show the best performance in tensile strength and elongation at break. The performance gradually decreases with further addition of organoclays. In contrast to the tensile strength and elongation at break, the elastic modulus of the nanocomposites is always enhanced by additions of the organoclays. These observations illustrate that the TPU/organoclay nanocomposites have improved elasticity and elastic modulus after being mixed with a small amount of organoclay. These changes are due to the ability of the clay silicate layers to strengthen, stiffen, and toughen the TPU matrix. With higher organoclay contents, the dispersion of silicate layers decreases, and the organoclay silicate layers tend to form agglomerates rather than exfoliate. This leads to poor interfacial adhesion between the TPU matrix and the filler phases, and thus reduced performance. Consequently, the nanocomposites tend to become rigid and brittle materials. Mechanical properties of the nanocomposites show the following order: TPU/I.34TCN ≥ TPU/I.30P > TPU/I.28E > TPU/I.44P. The greater mechanical reinforcement of the TPU/I.34TCN and TPU/I.30P nanocomposites is also due to the strong interfacial interaction between the silicate layers and TPU matrix. This forms a network-like structure, which causes improved mobility of the silicate layers during the deformation of the TPU matrix. This consequently further improves the break energy and improves the mechanical properties of the TPU/organoclay nanocomposites [9].

Oxygen gas permeability

Films of neat TPU and TPU/organoclay nanocomposites with 60–80-μm thickness are blown to evaluate the oxygen gas permeability. The relative permeability (P_r) is generally expressed as a barrier improvement compared with pristine TPU. This is calculated according to the following equation:

$$P_r = \frac{P_s}{P_p} \tag{1}$$

where P_s and P_p represent the permeability of the composite film and that of the pure polymer. Nielsen's model [32, 33] of barrier properties is employed to describe the relationship between the aspect ratio of the silicate layer agglomerates and the enhancement in barrier properties of the nanocomposites. The impermeable silicate layers act as a barrier to gas diffusion by increasing the tortuousness of the diffusion pathway. The permeability can be estimated from the equation,

$$P_r = \frac{P_s}{P_p} = \frac{1 - \phi_S}{1 + \frac{\alpha}{2}\phi_S} \tag{2}$$

where α is the aspect ratio of the silicate layer agglomerates in the polymer matrix, representing a comparison of length to width; ϕ_S is the volume fraction, calculated using the equation [34]

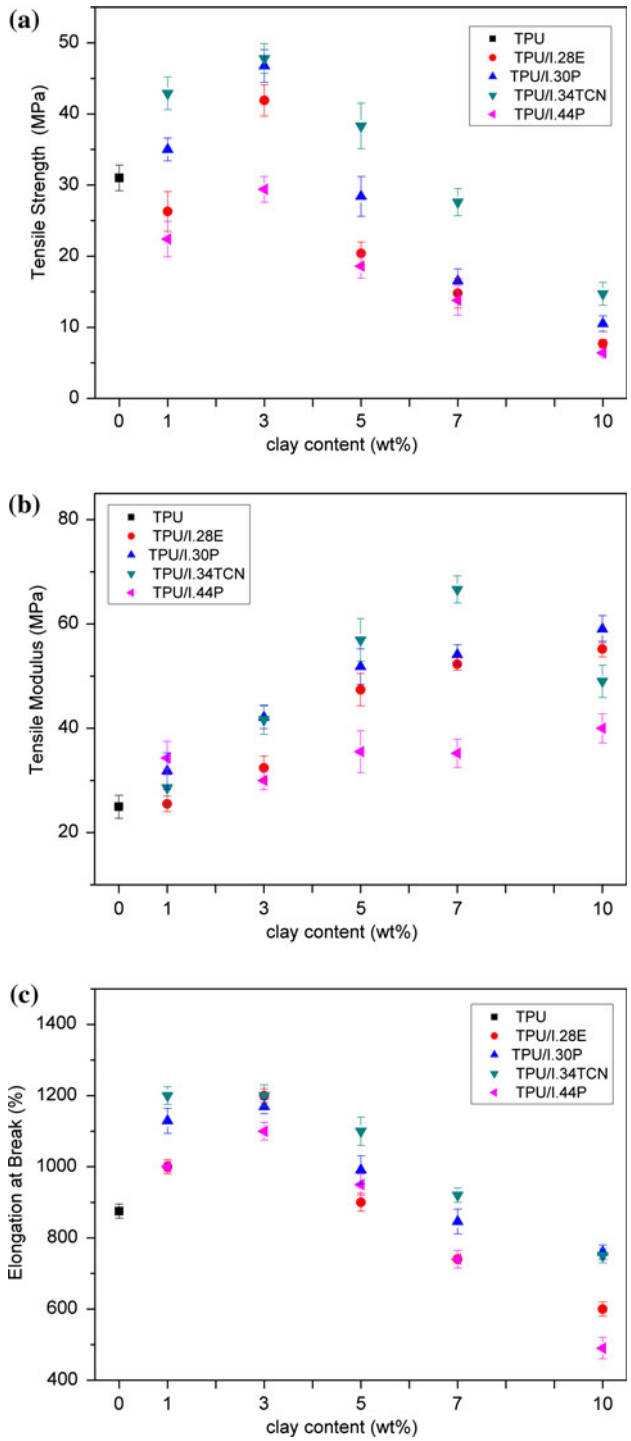

Fig. 8 Tensile properties of TPU nanocomposites with **a** tensile strength, **b** elastic modulus, and **c** elongation at break

$$\phi_S = \frac{1}{1 + \frac{\rho_s(1-M_c)}{\rho_p M_c}} \tag{3}$$

where ρ_s and ρ_p are the densities of the organoclay and the polymer, respectively, and M_c is the mass fraction of clay. Table 2 shows the aspect ratio calculated by fitting the permeation data obtained experimentally to Nielsen's model and statistics from the TEM images. The fitted α for most of the clay series is slightly lower than the statistical values from the TEM images.

As shown in Fig. 9, the relative permeability decays asymptotically with increasing clay loading. A 35–40% reduction of permeability was obtained with 10 wt% of all types of organoclay. The dotted lines fitted by the Nielsen's model with α of 15, 20, 35, and 50 are also illustrated in Fig. 9. These slightly fit the relative permeability of TPU/I.44P, TPU/I.28E, TPU/I.30P, and TPU/I.34TCN, respectively. Moreover, the TPU/I.34TCN and TPU/I.30P nanocomposites show better gas barrier property than do TPU/I.28E or TPU/I.44P. This behavior may be due to better dispersion of organoclay and the higher α of the silicate layer agglomerates in TPU/I.34TCN and TPU/I.30P [35, 36].

Hydrogen bonding

FTIR spectroscopy is performed to see if the improved organoclay dispersion and tensile and gas barrier properties are due to the interaction between hydroxyl groups/ammonium ions in the clays and the TPU matrix [37, 38]. The FTIR spectra of neat TPU and TPU/organoclay nanocomposites with 5 wt% clay are shown in Fig. 10. The absorption peak at 3320 cm^{-1} is due to the hydrogen-bonded –NH groups of urethane linkages. Such hydrogen bonding can be formed with carbonyl and with ether linkages. The peak at 1730–1735 cm^{-1} is assigned to free urethane carbonyl, and that at 1700–1705 cm^{-1} is due to hydrogen-bonded carbonyl [39]. The ratio of area under the hydrogen-bonded carbonyl peak (A_{HCO}) to that of the free carbonyl peaks (A_{FCO}) and the ratio of the area under the peaks of hydrogen-bonded –NH groups (A_{HNH}) to that of the –CH stretching peak (A_{CH}, 2800–3000 cm^{-1}) are shown in Table 3. The value of A_{CH} was used as the reference value. Notably, the value of A_{HNH}/A_{CH} of the TPU/organoclay nanocomposites is almost unchanged, which indicates that silicate layers do not interfere with hydrogen bonding between urethane and –NH groups. The values of A_{HCO}/A_{FCO} of TPU/I.30P and TPU/I.34TCN are higher, whereas that of TPU/I.28E is very close to that of pure TPU, and that of TPU/I.44P is lower than the ratio for pristine TPU. This result is due to the hydrogen bonding between hydroxyls/ammonium ions in the silicate layers and the carbonyls of TPU, which influences the exfoliation and dispersion of silicate layers in the TPU and greatly improves the mechanical and gas barrier properties.

Conclusions

TPU/organoclay nanocomposites with different organoclay loadings have been prepared by a melt extrusion process

Table 2 Aspect ratio of the silicate layer agglomerates in TPU nanocomposites with 3 and 7 wt% clay

	I.28E		I.30P		I.34TCN		I.44P	
Clay content (wt%)	3	7	3	7	3	7	3	7
Clay volume fraction	0.017	0.040	0.017	0.040	0.017	0.040	0.017	0.040
Aspect ratio[a]	21	20	35	19	42	29	16	14
Aspect ratio[b]	27	21	30	26	47	42	6	8

[a] Fitted by the Nielsen's model

[b] Statistical data from TEM photos

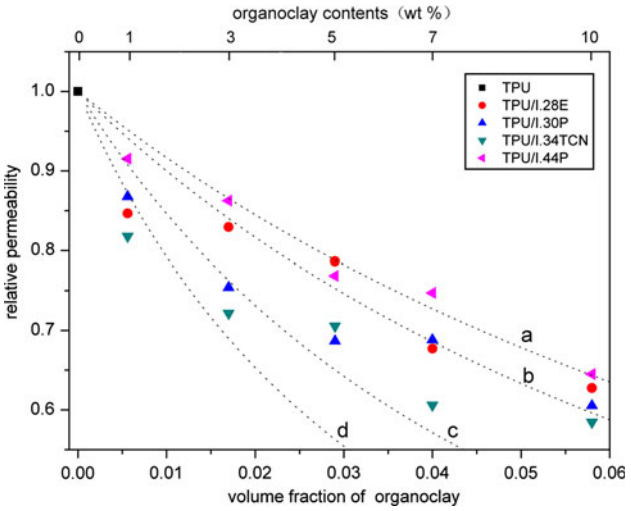

Fig. 9 Oxygen gas permeability of TPU nanocomposites. The *dotted lines* were fitted by the Nielsen's model with aspect ratio of (*a*) 15, (*b*) 20, (*c*) 35, and (*d*) 50

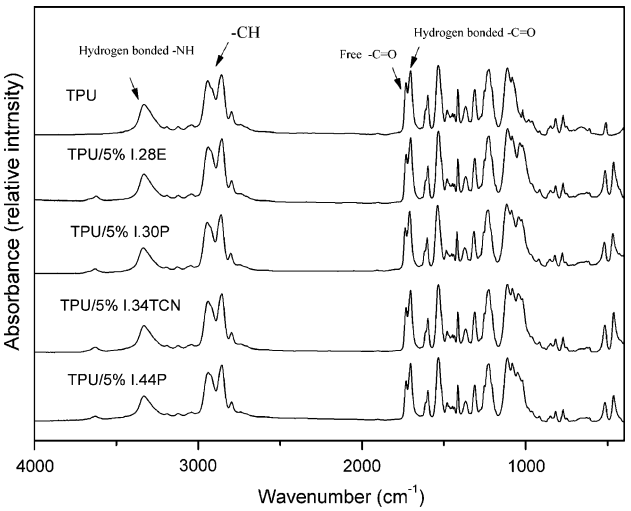

Fig. 10 FTIR spectra of pure TPU and TPU/organoclay nanocomposites with 5 wt% clay

using a twin-screw extruder. The influence of organoclays with various organic modifiers on the morphology and mechanical properties of the nanocomposites have been explored. Four types of organoclays were used, namely, I.28E, I.30P, I.34TCN, and I.44P. The WAXD and TEM results illustrate that the I.34TCN and I.30P show greater dispersion and exfoliation of silicate layers than do I.28E or I.44P. This is due to the strong interaction between the polyurethane chain and the organic modifiers used in I.34TCN and I.30P. This interaction also enhances the interaction between the silicate layers and TPU matrix, and further influences the mechanical properties and gas permeability of the nanocomposites. The FTIR spectra indicate that the interaction is due to hydrogen bonding between hydroxyls/ammonium ions in the silicate layers and carbonyls of TPU. At greater organoclay loading (particularly at >3 wt%), the dispersion of silicate layers decreases, and the organoclay silicate layers tend to agglomerate rather than exfoliate. This reduces the enhancement of the mechanical properties. Moreover, the mechanical and gas barrier properties of the nanocomposites follow the order TPU/I.34TCN ≥ TPU/I.30P > TPU/I.28E > TPU/I.44P. The TPU/I.34TCN and TPU/I.30P nanocomposites display lower T_g and higher G', compared with those of TPU/I.28E and TPU/I.44P.

Table 3 Ratio of the area under the absorption peaks of hydrogen-bonded C=O (A_{HCO}) and free C=O (A_{FCO}) groups, and ratio of the area under the peaks of hydrogen-bonded –NH (A_{HNH}) and –CH stretching (A_{CH}) in the FTIR spectra

	TPU	TPU/ I.28E	TPU/ I.30P	TPU/ I.34TCN	TPU/ I.44P
A_{HCO}/A_{FCO}	2.23	2.25	2.29	2.32	2.05
A_{HNH}/A_{CH}	0.33	0.31	0.33	0.31	0.32

References

1. Kawasumi M, Hasegawa N, Kato M, Usuki A, Okada A (1997) Macromolecules 30:6333
2. Usuki A, Kojima Y, Kawasumi M et al (1993) J Mater Res 8:1179
3. Zhong Y, Zhu ZY, Wang SQ (2005) Polymer 46:3006. doi: 10.1016/j.polymer.2005.02.014
4. Chang JH, An YU, Sur GS (2003) J Polym Sci B Polym Phys 41:94. doi:10.1002/polb.10349

5. Jeong HM, Kim BC, Kim EH (2005) J Mater Sci 40:3783. doi:10.1007/s10853-005-3719-4
6. Zhang YD, Liu QF, Zhang QA, Lu YP (2010) Appl Clay Sci 50:255. doi:10.1016/j.clay.2010.08.006
7. Oral A, Tasdelen MA, Demirel AL, Yagci Y (2009) Polymer 50:3905. doi:10.1016/j.polymer.2009.06.020
8. Ramazani SAA, Tavakolzadeh F, Baniasadi H (2010) J Appl Polym Sci 115:308. doi:10.1002/app.31102
9. Ren CY, Jiang ZY, Du XH, Men YF, Tang T (2009) J Phys Chem B 113:14118. doi:10.1021/jp9063164
10. Ray SS, Okamoto M (2003) Prog Polym Sci 28:1539. doi:10.1016/j.progpolymsci.2003.08.002
11. Zha WB, Han CD, Han SH et al (2009) Polymer 50:2411. doi:10.1016/j.polymer.2009.03.018
12. Yang M, Wang P, Huang CY, Ku MS, Liu HJ, Gogos C (2010) Int J Pharm 395:53. doi:10.1016/j.ijpharm.2010.04.033
13. Simons R, Qiao GG, Powell CE, Bateman SA (2010) Langmuir 26:9023. doi:10.1021/la904827d
14. Tian Y, Yu H, Wu SS, Ji GD (2004) J Mater Sci 39:4301. doi:10.1023/B:JMSC.0000033412.92494.ee
15. Lakshminarayanan S, Lin B, Gelves GA, Sundararaj U (2009) J Appl Polym Sci 112:3597. doi:10.1002/app.29679
16. Krishnamoorti R, Vaia RA, Giannelis EP (1996) Chem Mater 8:1728
17. Giannelis EP (1996) Adv Mater 8:29
18. Wang Z, Pinnavaia TJ (1998) Chem Mater 10:3769
19. Tien YI, Wei KH (2001) Macromolecules 34:9045. doi:10.1021/ma010551p
20. Cai YB, Hu Y, Song L et al (2007) J Mater Sci 42:5785. doi:10.1007/s10853-006-0634-2
21. Pegoretti A, Dorigato A, Brugnara M, Penati A (2008) Eur Polym J 44:1662. doi:10.1016/j.eurpolymj.2008.04.011
22. Dan CH, Kim YD, Lee MH, Min BH, Kim JH (2008) J Appl Polym Sci 108:2128. doi:10.1002/app.27879
23. Dan CH, Lee MH, Kim YD, Min BH, Kim JH (2006) Polymer 47:6718. doi:10.1016/j.polymer.2006.07.052
24. Cipriano BH, Kota AK, Gershon AL et al (2008) Polymer 49:4846. doi:10.1016/j.polymer.2008.08.057
25. Calcagno CIW, Mariani CM, Teixeira SR, Mauler RS (2007) Polymer 48:966. doi:10.1016/j.polymer.2006.12.044
26. Lee MH, Dan CH, Kim JH et al (2006) Polymer 47:4359. doi:10.1016/j.polymer.2006.04.003
27. Jia QM, Zheng M, Zhu YC, Li JB, Xu CZ (2007) Eur Polym J 43:35. doi:10.1016/j.eurpolymj.2006.10.016
28. Balazs AC, Singh C, Zhulina E (1998) Macromolecules 31:8370
29. Lyatskaya Y, Balazs AC (1998) Macromolecules 31:6676
30. Worzakowska M (2009) J Mater Sci 44:4069. doi:10.1007/s10853-009-3587-4
31. Meng XY, Wang Z, Zhao ZF, Du XH, WG Bi, Tang T (2007) Polymer 48:2508. doi:10.1016/j.polymer.2007.03.009
32. Nielsen LE (1967) J Macromol Sci Chem A1:929
33. Lan T, Kaviratna PD, Pinnavaia TJ (1994) Chem Mater 6:573
34. Chen BQ, Evans JRG (2006) Macromolecules 39:747. doi:10.1021/ma052154a
35. Chang JH, An YU, Cho DH, Giannelis EP (2003) Polymer 44:3715. doi:10.1016/s0032-3861(03)00276-3
36. Osman MA, Mittal V, Morbidelli M, Suter UW (2003) Macromolecules 36:9851. doi:10.1021/ma035077x
37. Pattanayak A, Jana SC (2005) Polymer 46:5183. doi:10.1016/j.polymer.2005.04.035
38. Pattanayak A, Jana SC (2005) Polymer 46:3275. doi:10.1016/j.polymer.2005.02.081
39. Kim W, Chung DW, Kim JH (2008) J Appl Polym Sci 110:3209. doi:10.1002/app.28929